# Large Plastic Deformation of Isotactic Poly(propylene) (iPP) Evaluated by WAXD Techniques

*Dimitrios Samios,* Shinichi Tokumoto, Elton L. G. Denardin*

**Summary:** Commercial isotactic poly(propylene) (iPP), obtained in bars, was annealed and submitted to different levels of plastic deformation by uniaxial plane compression using a special device which permits well controlled temperature and strain rate. The evolution of the microstructure was followed at different degrees of deformation by wide angle x-ray diffraction (WAXD) techniques. The spherulite fragmentation process, lamellar orientation and destruction of the crystallites is argued, according to collected analytical data in the flow direction (FD), the loading direction (LD) and the lateral or constrain direction (CD). The evaluation of the WAXD patterns in terms of diffraction line position, intensity and width, permits to affirm that, while the large plastic deformation occurs, the crystalline net suffers anisotropic deformation, the crystallites become preferentially oriented along the flow direction and the crystalline phase diminish in amount indicating lesser and smaller crystallites. The gradual lamellae fragmentation occurs, starting with apparent crystalline size of approximately 30 nm for the non-deformed material and gradually decreasing to approximately 15 nm for the 70% deformed one.

**Keywords:** large deformation; poly(propylene); WAXD

## Introduction

There were numerous studies on the thermo-mechanical behavior of iPP owing to the large number of applications of the material. In the last 30 years, iPP was studies in view of understanding microstructure or mechanical behavior. The organization of the crystalline phases of iPP, α-monoclinic, β-hexagonal and γ-triclinic have been reported in literature[1–4] as well as Natta and Corradini[5] reported a mesomorphic smetic phase.[6,7]

The process of the plastic deformation is present in the diverse forms of current plastic transformation, as thermo processing, molding and stretching of fibers and oriented films.[8] The initial studies concerning the morphological changes in semicrystalline polymers, after the deformation by stress application were made by Flory and Yoon[9] and Peterlin.[10] Galeski et al.[11] reported that the initial spherulitic morphology is destroyed and transformed into stacks of crystalline lamellae with their normal rotating towards the load direction, while the chain axis tends toward the flow direction. Different studies have explored deformation at temperatures above and next to the glass transition temperature ($T_g$), however below the fusion temperature ($T_m$). Detailed investigations of the mechanisms of plastic deformation have been reported by Cohen et al.[12–14] for semi-crystalline polymers as nylon, poly(ethylene terephthalate) (PET) and high density polyethylene (HDPE). In general forms, microstructural changes in the levels of spherulites, lamella and amorphous phase[15–17] have been observed.

The present study aims to expand the knowledge of morphological properties of iPP samples before and after deformation, prepared by plane strain compression. The

Laboratório de Instrumentação e Dinâmica Molecular, Instituto de Química-UFRGS, Av. Bento Gonçalves, 9500, C.P. 15003, Porto Alegre-RS, CEP 91501-970, Brazil
E-mail: dsamios@iq.ufrgs.br

plastic deformation promoted by compression in channel die[18] has the advantage of getting samples without cavitations, moreover, contrary to the drawing, the compression experiments permit application of extremely high stresses with consequently strong changes of the material texture and morphology.[19,20] Additionally, as it is going to be demonstrated, the use of WAXD techniques for the characterization of the samples before and after deformation contributes to the elucidation of effects caused by the large plastic deformation process, approaching orientation and modification of the micro and nano structural properties, specially the α-monoclinic organization and the amorphous ''halo'' obtained and described in various studies.[17,21]

## Experimental Part

The device used for the deformation of the iPP samples is a force amplifier developed for compression tests, which is covered by our patent deposit number BR7903031-9[22] coupled in to the Instron® dynamometer Model 4466, equipped with 10 kN compression-tension cell. The system is based on Pascal's principle, with two hydraulic cylinders interconnected by stainless steel tubing. The force amplification is determined by area ratio of the transversal section between secondary and primary piston. Force magnification of 22:1 was suitable for the present purpose. More details about the experimental device are given by Tokumoto.[23]

One of the most important advantages is the magnification of discrete deformational events. Displacement on secondary piston, which corresponds directly to specimen deformation, is as small as the inverse of force magnification. Once displacement is measured in the primary piston, material response is spread in a wide range. The mould plunger and the channel are demonstrated in Figure 1.

A commercial sample of iPP H503, produced by OPP Química S.A. and stabilized with antioxidant and antacid substances, was used to obtain bars of 12.5 mm × 6.35 mm × 100 mm by molding injection using the injector Batenfeld Sb1450-230/4001 model. The injection conditions have been adjusted so that the material with molecular weight $M_w =$ 419.800 and $M_w/M_n = 7.6$ was processed without leaving bubbles or sink marks in the sample. The prepared bars have been annealed in vacuum oven with temperature of $140 \pm 5\,^{\circ}C$ for 6 h, previously purged with nitrogen.

The specimen was laid on the bottom of channel die, which exhibits dimensions of 6.35 mm in width, 20.00 mm in height and 100.00 mm in length, and sandwiched with 45 mm length plunger, as schematized in Figure 1. The temperature of the specimen was controlled by circulating silicone oil pumped from thermostatic bath, which passes through five holes in the die body around the channel. The thermocouple was placed in a small hole just below the bottom of the channel.

Test parameters other than channel temperature were controlled in the primary piston by Instron® model 4466 dynamometer: load value, compression speed and displacement. Three groups of deformed samples with final deformation of 10, 45 and 70% were prepared at the temperature of $70\,^{\circ}C$ and compression rate of $1.8\ mm \cdot min^{-1}$.

### Analysis by Wide Angle x-ray Diffraction– (WAXD)

The non-deformed and the plastically deformed samples of isotactic poly(propylene) were analyzed by WAXD in the three faces, as shown in Figure 1.

The crystallographic planes of the materials have been evaluated by Rigaku x-rays diffractometer, D/MAX-2100 model, with goniometer ''Ultima+'' type theta-theta and NaI scintillate detector. The pipe, with copper anode, was used as source of x-rays Cu Kα with $\lambda = 1.54$ Å. Work tension of 40 kV and current of 26 mA have been applied in the scanning, carried through speed of $2^{\circ}\ min^{-1}$ and step of $0.02^{\circ}$. The angular scanning covered the band of $7^{\circ}$ to

 

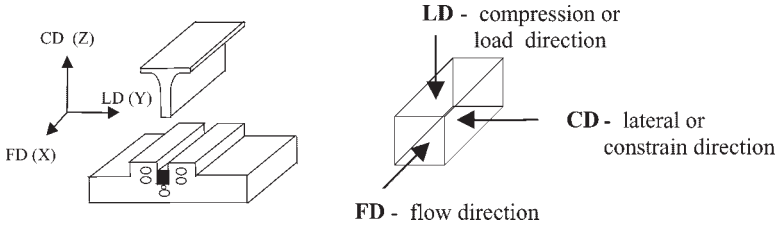


***Figure 1.***
The channel, the plunger and the sample.

60°, being overcome its diffraction of the reflected rays. In FD face, which has a small superficial area, the scanning speed was of $0.5^\circ\ \text{min}^{-1}$.

Generally, according to the superposition theorem:[24] the measured profile h(e) of a diffraction line is the result of the convolution of the pure line profile f(e) and the profile instrumental function g(e) as given by Equation (1).

$$h(e) = \int_{-\infty}^{+\infty} g(\eta(\eta)f - \eta)d\eta \tag{1}$$

The intensity of the diffracted lines of a determined crystallographic plane (*hkl*) and single phase depends on the following factors, according to Equation (2):

$$I_{(hkl)} \propto \frac{m^2_{(hkl)}}{\mu V^2}\left|F_{(hkl)}\right|^2 \frac{1}{\sin^2\theta\cos\theta} \times (1+\cos^2 2\theta)\mathrm{P}_\alpha(2\theta) \tag{2}$$

where $m$ = multiplicity factor of the plan (*hkl*); $\mu$ = linear absorption coefficient; $V$ = unitary cell volume; $F(hkl)$ = structure factor; $1/(\sin^2\theta\ \cos\ \theta)$ = Lorentz factor; $P_\alpha(2\theta)$ = texturization factor; $(1+\cos^2 2\theta)$ = factor of polarization for diffractometer without monocromator.

Here, the intensity of the diffracted rays of iPP is studied in relation to the effect of the texturization and the Lorentz phenomena. The instrumental function of the diffractometer was obtained by analysis of standard $LaB_6$ sample, analyzed under the same conditions of the iPP samples. In order to obtain the pure line profile f(e) it is necessary to deconvolute the instrumental function g(e) from the measured profile h(e).

For simplification of the deconvolution of the functions analytical Lorentz functions were used, with the use of the Fourier transformation, for the instrumental profile and the pure line profile. The consideration is reasonable, because the analytical adjustment of the lines of the standard $LaB_6$ sample, as well as the measured total profile of the iPP samples, with Lorentz functions showed satisfactory results. Additionally, the fitting of the curves through Lorentz functions showed better results than that of the Gauss functions. In this way, the total width of measured diffraction profile can be regarded as the simple addition of the contribution of the width of the instrumental function and that of the sample line.

The contribution of crystals with small dimensions to the width has origin in the rays with small deviation in relation to condition of Bragg diffraction, which are detected by not finding the respective pairs for destructive interference. These last ones would have origin in the reflection in deeper planes, which does not exist in function of the limited dimensions of the crystal. The widening for this factor is expressed for

$$\Delta\theta = \lambda/[4L\cos\theta_\mathrm{B}] \tag{3}$$

or rearranging

$$L = K\lambda/B_\mathrm{ob}\cos\theta \tag{4}$$

where $L$ is the crystal dimension, $K$ the Scherrer factor and $B_\mathrm{ob}$ the obtained line width.

In practice, crystals with thickness of 1 000 Å behave as infinite crystals and do not contribute to the widening. Opportunely, considering that the crystalline

 

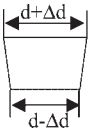


A dimension d of the unitary cell of the crystalline net under tension $\Delta d/d = 2\varepsilon$, where $\varepsilon$ is the deformation

***Figure 2.***
Deformation of unitary cell.

thickness of lamellae of iPP vary approximately from 50 to 500 Å,[25,26] it makes the x-ray diffraction a useful technique for evaluation of the crystalline modification of the thickness of iPP lamellae with the plastic deformation.

The process of the plastic deformation can cause also the deformation of the crystalline net as shown in Figure 2, which contributes to the width of the diffraction peak. The deformation of the net is understood here as being a microscopic deformation, where the Hooke law is again valid.

Equation (5) defines the widening caused by deformation of the net.

$$\frac{\Delta d}{d} = -\frac{\cos\theta}{\sin\theta} = -\frac{\Delta\theta}{\tan\theta} = -\frac{\Delta 2\theta}{2\tan\theta} = 2\varepsilon \quad (5)$$

A new parameter can be defined by the Equation (6).

$$s = 2\sin\theta/\lambda \quad (6)$$

and consequently:

$$\Delta s = (2/\lambda)\cos\theta\Delta\theta \quad (7)$$

Considering Lorentz profile the total width is given by Equation (8).

$$B(s) = B(s)_{\text{dimensional}} + B(s)_{\text{deformational}} = K/L + 2\varepsilon s \quad (8)$$

or

$$B_{\text{ob}} = (B_{\text{dim}}/\lambda)\cos\theta + 2\varepsilon(2\sin\theta/\lambda) \quad (9)$$

where $B_{\text{ob}}$ is the width obtained after deconvolution.

Equation (9) is a linear function of the s parameter. Taking into account the small values of $\theta$, the plot of $B_{\text{ob}}$ versus $s$ can, theoretically, reveal the dimensional and deformational contributions to the total width. Extrapolation of the obtained curves to $\theta = 0$ ($s = 0$, $\sin\theta = 0$, $\cos\theta = 1$) enables to obtain the size of the crystallites. However, the validity of Equation (8) and (9) is strong argued in semicrystalline polymer systems which are normally considered as a combination of an amorphous phase and a crystalline one. The equation was developed for polycrystalline materials and the parameters obtained by extrapolation to zero s value in polymer semicrystalline systems are characterized by strong uncertainty.

## Results and Discussion

Figure 3 shows three groups of x-ray diffraction patterns of iPP-H5 samples in the loading (LD), the constrain (CD) and

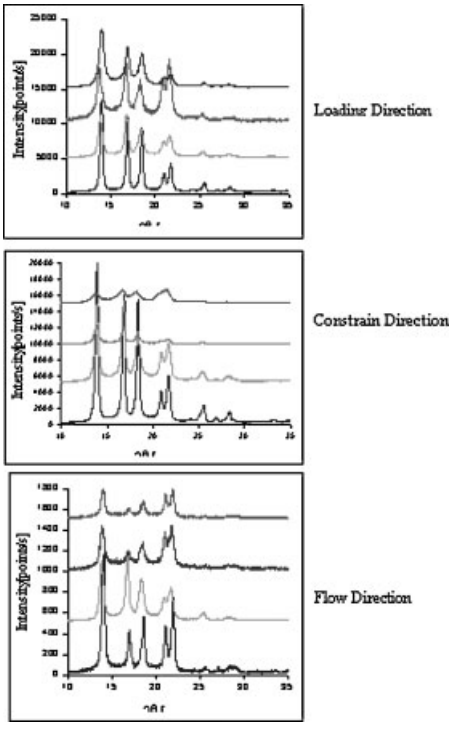


***Figure 3.***
X-ray diffraction patterns of specimens from sample iPP-H5. Nominal compression ratio of 0, 10, 45 and 70% are represented on the plots, from the bottom to the top, respectively. Compressions where performed at 70 °C and 1.8 mm · min$^{-1}$ compression rate.

 

the flow (FD) direction, respectively. The compression ratios of 0, 10, 45 and 70% are shown as indicated in the plots. The deformations were performed at 70 °C and 1.8 $mm \cdot min^{-1}$ constant compression rate.

As all ready presented in other papers,[17,21] the x-ray diffraction patterns have been fitted according to the two phase model which considers the semicrystalline system as composed by the amorphous and the crystalline phases. The results of the fitting procedures are summarized in Table 1. In this table, for every diffraction peak, characterized by the corresponding diffraction plane (*hkl*), are given the peak maximum position ($2\theta$), the normalized integrated intensity ($I$) and the width at half high ($2\Gamma$). The table includes the data for the non-deformed (0%) and the deformed samples with 10, 45 and 70% compression ratios. The values of the apparent relative crystallinity (RCr) are shown in Table 2. The following discussion aims to elucidate morphological changes in the material during the deformation process by plane compression. This way, both, order and disorder of the semicrystalline material have to be considered.

The order-disorder question of semicrystalline polymers can be analyzed according to two aspects.[7] The first one, is related to the size of the crystallites. The higher aggregates correspond to the crystallites of higher dimensions, and they contribute for the well defined x-ray diffraction peaks. The amorphous phase is interpreted according to two main interpretations: the first one[27–30] considers a completely random arrangement of the polymeric chains, the second[31,32] assumes the existence of organization of short range order, even so highly disturbed. More recently,[33,34] studies with techniques such as scanning electronic microscopy and electron diffraction have revealed that the second hypothesis is more consistent. Thus, the amorphous phase can also be known as micro or nanocrystalline phase. The second aspect refers to the paracrystalline disorder of the material[35] which again is related to the micro and nanocrystallites. In fact, the dimension of a crystallite is determined by the extension of the paracrystalline fluctuations.

As discussed in previous publications,[16,19] in the case of iPP the evolution of the process of plastic deformation causes

***Table 1.***
Numerical results of the evaluation of the iPP-H5 WAXD diffraction patterns.

| CR | (*hkl*) | FD | | | LD | | | CD | | |
|---|---|---|---|---|---|---|---|---|---|---|
| | | $2\theta$ | I | $2\Gamma$ | $2\theta$ | I | $2\Gamma$ | $2\theta$ | I | $2\Gamma$ |
| | 110 | 14.02 | 0.24 | 0.27 | 13.90 | 0.23 | 0.27 | 14.00 | 0.24 | 0.25 |
| | 040 | 16.95 | 0.08 | 0.29 | 16.80 | 0.22 | 0.29 | 16.90 | 0.23 | 0.27 |
| 0% | 130 | 18.50 | 0.11 | 0.26 | 18.37 | 0.19 | 0.29 | 18.45 | 0.21 | 0.28 |
| | 111 | 21.05 | 0.13 | 0.26 | 20.82 | 0.05 | 0.40 | 20.92 | 0.04 | 0.40 |
| | 041+131 | 21.88 | 0.19 | 0.30 | 21.70 | 0.09 | 0.35 | 21.78 | 0.08 | 0.33 |
| | 110 | 13.90 | 0.27 | 0.37 | 13.88 | 0.17 | 0.36 | 13.85 | 0.19 | 0.38 |
| | 040 | 16.80 | 0.06 | 0.35 | 16.75 | 0.19 | 0.37 | 16.75 | 0.23 | 0.40 |
| 10% | 130 | 18.35 | 0.08 | 0.40 | 18.33 | 0.13 | 0.52 | 18.30 | 0.16 | 0.55 |
| | 111 | 20.95 | 0.10 | 0.41 | 20.90 | 0.09 | 0.55 | 20.83 | 0.02 | 0.59 |
| | 041+131 | 21.75 | 0.14 | 0.46 | 21.73 | 0.09 | 0.52 | 21.73 | 0.06 | 0.54 |
| | 110 | 13.91 | 0.13 | 0.42 | 13.85 | 0.19 | 0.41 | 13.74 | 0.11 | 0.49 |
| | 040 | 16.80 | 0.04 | 0.45 | 16.70 | 0.16 | 0.42 | 16.65 | 0.11 | 0.40 |
| 45% | 130 | 18.44 | 0.08 | 0.44 | 18.30 | 0.11 | 0.53 | 18.25 | 0.09 | 0.55 |
| | 111 | 20.95 | 0.15 | 0.51 | 20.82 | 0.06 | 0.57 | 20.70 | 0.13 | 0.57 |
| | 041+131 | 21.87 | 0.18 | 0.52 | 21.71 | 0.06 | 0.47 | 21.70 | 0.15 | 0.54 |
| | 110 | 13.97 | 0.11 | 0.39 | 13.66 | 0.07 | 0.75 | 14.00 | 0.22 | 0.55 |
| | 040 | 16.90 | 0.02 | 0.47 | 16.60 | 0.09 | 0.80 | 16.90 | 0.15 | 0.53 |
| 70% | 130 | 18.50 | 0.08 | 0.43 | 18.22 | 0.11 | 0.82 | 18.45 | 0.15 | 0.57 |
| | 111 | 21.07 | 0.15 | 0.48 | 20.55 | 0.07 | 0.58 | 20.95 | 0.02 | 0.54 |
| | 041+131 | 21.89 | 0.18 | 0.45 | 21.55 | 0.16 | 0.65 | 21.85 | 0.03 | 0.56 |

 

*Table 2.*
Relative apparent crystallinity results obtained by evaluation of the WAXD patterns.

| Compression ratio | $RCr_{LD}$ | $RCr_{CD}$ | $RCr_{FD}$ |
|---|---|---|---|
| % | % | % | % |
| 0 | 0.80 | 0.78 | 0.76 |
| 10 | 0.66 | 0.66 | 0.65 |
| 45 | 0.59 | 0.58 | 0.58 |
| 70 | 0.57 | 0.48 | 0.54 |

an increase of the reflections of the microcrystalline or amorphous phase, the so named ''amorphous halo'' of the diffraction pattern. The same behavior is shown in Table 2 with respect to the ''amorphous halo''. This is due to the fact that the organization of the crystallites are gradually destroyed, increasing the fraction of the material with deficient organization. The reflections of this phase were found between 15° and 21.5°, below the crystalline peaks, as shown in Figure 3.

We must have in mind that this increase occurred to the detriment of the crystalline reflections resulted in the reduction of the density of the material, evaluated in a density gradient column and the crystallinity measured by DSC.[21] According to Table 2 the apparent relative crystalline fractions (RCr) along the three deformation axes, namely LD, CD and FD present practically comparable values and the decrease with the deformation is practically the same. However, taking a nearer look, we observe that this decrease occurred differently in the different crystallographic planes. The elucidation of this phenomenon can be possible by a deeper analysis of the crystallographic characteristics of the iPP, specially the planes (110), (040), (130), (111), (041) and (131) which mainly contribute to the diffraction patterns.

The α-monoclinic structure of iPP is identified in literature[36] as becoming to the space group $P2_1/c$ and it has been referenced by recent study.[7] It is well known that in the iPP α-monoclinic structure the ellipsis-chain segments are approximately perpendicular to the crystalline surface of lamellae.[25] The crystallographic c-axis is oriented parallel to the ellipsis-chain segments.[25] The main crystallographic planes of iPP can be mainly divided in two groups, namely group-**a** including the planes (110), (040) and (130) which are normal to the (001). The planes are parallel to the crystallographic c-axis and consequently parallel to the ellipsis-chain segments. Group-**b** includes the planes (111), (041) and (131) which are inclined in relation to the surface of lamellae. The planes (041) and (131) appear together in the diffraction pattern and it is not possible to separate their contributions. These characteristics enable the adequate definition of orientation parameters which can be used to elucidate the orientation and the reorientation of structural elements during the compression deformation process. In this study, considering the characteristics of the planes, we defined the orientation parameters given by the relation

$$A_{hkl/jnm} = [I_{hkl}]/[I_{hkl} + I_{jnm}] \quad (10)$$

The values and the behavior of the orientation parameter $A_{hkl/jnm}$ depend on the intrinsic intensities of the crystallographic planes (*hkl*) and (*jnm*), the choice of the experimental diffractometer geometry, namely LD, CD or FD and is related to the variation of the structural elements orientation caused by rotation, dislocation or even deformation, fragmentation and amorphisation of the them. The obtained orientation parameters are given in Table 3.

The variation of the $A_{040/110}$ parameter is related to the rotation of the crystallites along the c-axis. With respect to $A_{040/111}$ parameter, the rotation is along the direction defined by the axis A = 1 and B = 1. If the crystallites are isotropically distributed, the orientation parameters obtained in LD, CD and FD directions have to be equal.

The evaluation of the relative intensities, Table 1, the comparable relative intensities of the group-**a** planes along LD and CD and the characteristics of the planes described above, as well as, the orientation parameters, Table 3, indicate that in the

 

*Table 3.*
Orientation parameters of the iPP-H5 samples, deformed at 70 °C.

| Parameter $A_{hkl/jmn}$ | $A_{040/110}$ | | | $A_{130/110}$ | | | $A_{110/111}$ | | |
|---|---|---|---|---|---|---|---|---|---|
| CR (%) | LD | CD | FD | LD | CD | FD | LD | CD | FD |
| 00 | 0.48 | 0.50 | 0.25 | 0.45 | 0.46 | 0.31 | 0.81 | 0.85 | 0.65 |
| 10 | 0.53 | 0.53 | 0.18 | 0.43 | 0.46 | 0.23 | 0.66 | 0.88 | 0.72 |
| 45 | 0.47 | 0.50 | 0.23 | 0.37 | 0.45 | 0.38 | 0.75 | 0.48 | 0.47 |
| 70 | 0.54 | 0.42 | 0.15 | 0.61 | 0.40 | 0.42 | 0.50 | 0.91 | 0.42 |

initial samples there is an orientation along the injection direction and consequently a significant axial orientation along the FD direction. A narrow look to the evolution of the different intensities in the flow direction FD shows a strong decrease in the group-**a** peaks.

The (040) peak practically disappears in the 70% diffraction pattern and the (110) and (130) planes after a drastic reduction. Contrary to the relative intensity decrease of the group-**a** peaks the group-**b** namely the (111), (041) and (131) planes show a strong relative intensity increase. The relative intensities evolution in the flow direction, reforced by the other two directions, suggests the orientation of the lamellae segments or fragments with the normal vectors to the surface of lamellae oriented parallel to the load direction. However, the evolution of the relative intensities cannot be justified by simple orientation arguments. The decrease of the crystalline part in Table 2 can only be understood if we consider the destruction of the spherulitic and lamellae structures and the accommodation of the lamellae fragments in the amorphous phase.

### Width of the Diffraction Profiles

Table 2 presents the obtained full widths at half maximum of the analyzed lines ($B_{ob} = 2\Gamma$). It can be observed that the plastic deformation promotes both processes in iPP, namely, crystalline net dimensional changes as well as deformation. The use of Equation (9) which considers a linear relationship between $B_{ob}$ and the dimensional and deformational contributions, and the extrapolation of the $B_{ob}$ to $s = 0.0$, according to this Equation, introduces an elevated uncertainty which does not permit the direct evaluation of these contributions. However, Equation (4) can be used in order to estimate the apparent crystalline size $L_{hkl}$ related to the dimension normal to the ($hkl$) plane. In the same way, using the width values ($2\Gamma$) of the Table 2, the average value $\langle B_{ob} \rangle$ can be obtained as the average of the five different planes and the corresponding average crystalline dimension $\langle L \rangle$ can be calculated according to Equation (4). Table 4 summarizes the crystalline net dimensions of the non-deformed and deformed iPP samples. Looking to the non-deformed samples, it can be verified that the $L_{110}$ corresponding crystalline size is approximately the same for FD, LD and CD directions, however the apparent average values of the $\langle L \rangle$ are smaller specially in the LD and CD directions which indicates deformational contribution to the loss of spatial coherence and consequently increase of the line width.

*Table 4.*
Crystalline size values obtained by analysis of the non-deformed and deformed iPP-H5 diffractional pattern line width analysis.

| Deformation (%) | | 0 | 10 | 45 | 70 |
|---|---|---|---|---|---|
| FD (X) | $L_{110}$/nm | 30.2 | 21.2 | $18.7 \pm 1.1$ | 20.1 |
| | $\langle L \rangle$/nm | $29.1 \pm 1.5$ | $19.7 \pm 2.4$ | $16.8 \pm 1.7$ | $17.6 \pm 2.1$ |
| LD (Z) | $L_{110}$/nm | 29.1 | 21.8 | 18.7 | 10.9 |
| | $\langle L \rangle$/nm | $24.6 \pm 2.9$ | $17.1 \pm 3.6$ | $16.4 \pm 2.8$ | $10.9 \pm 2.5$ |
| CD (Y) | $L_{110}$/nm | 32.7 | 20.7 | 16 | 14.3 |
| | $\langle L \rangle$/nm | $25.3 \pm 3.2$ | $16.0 \pm 3.5$ | $15.4 \pm 1.5$ | $14.3 \pm 1.4$ |

 

The evaluation of the variations of the $L_{110}$ with the different compression ratios indicates clearly a decrease with increasing deformation. The fragmentation of the lamellae structures and consequently the reduction of the crystallites size again are in agreement with the increase of the deformation. In the cases of 10% and 45% deformations the $\langle L \rangle$ values are smaller than the $L_{110}$ ones confirming the deformational contribution.

It is very important to observe that in 70% deformation the $L_{110}$ values, in the LD and CD axes, are significantly smaller than the initial dimension values, however the average crystalline size $\langle L \rangle$ values are very near to the obtained $L_{110}$ corresponding to crystalline size. A plausible explanation of this behavior is that, in the case of higher degrees of deformation of semicrystalline polymers, especially in the range after ''stress hardening point'' which is the case in 70% of the deformations, the deformation additionally to the orientation effects induces crystalline net modifications and measurable crystalline dimensional variation, in the case of iPP probably related to lamellae fragmentation.

## Conclusion

The evolutions of the structural elements orientation, as well as the modifications of the nano-structure for different degrees of deformation were evaluated. The evaluation of the WAXD patterns was performed relatively to the diffraction line position, the integrated intensity and the width, as well as the integrated intensity of the ''amorphous halo''. The realized analysis of the line integrated intensities and the orientations parameters demonstrated that the non-deformed iPP sample, even after annealing, presents axial orientation compatible with slight deformed spherulites. During the large plastic deformation, the crystalline net suffers anisotropic deformation, the crystallites become preferentially oriented along the flow direction and the crystalline phase diminish in amount indicating lesser and smaller crystallites. The apparent crystalline part is gradually reduced from 78 to 53%. The analysis of the line widths demonstrated that a gradual lamellae fragmentation occurs starting with apparent crystalline size of approximately 30 nm for the non-deformed material and decreasing to approximately 15 nm for the 70% deformed one.

*Acknowledgements:* The authors thank the *FAPERGS* and the *PADCT* for the financial support of this investigation.

[1] Z. Mencik, *J. Macromol. Sci., Phys.* **1972**, *B6*(1), 101.
[2] A. Turner-Jones, A. J. M. Cobbold, *J. Polym. Sci.* **1968**, *6*, 539.
[3] S. V. Meille, S. Bruckner, W. Porzio, *Macromolecules* **1990**, *23*, 4114.
[4] W. Xu, D. C. Martin, E. A. Arruda, *Polymer* **2005**, *46*(2), 455.
[5] G. Natta, P. Corradini, *Nuovo Cimento (Suppl.)* **1960**, *15*, 40.
[6] P. Zipper, A. Janosi, W. Geymayer, E. Ingolic, E. Fleischmann, *Polym. Eng. Sci.* **1996**, *36*(4), 467.
[7] A. Ferrero, E. Ferracini, A. Mazzavillani, V. Malta, *J. Macromol. Sci., Phys.* **2000**, *B39*(1), 109.
[8] *Modern Plastics Encyclopediax'92*, McGraw Hill, New York 1992, pp. 221–298.
[9] P. J. Flory, D. Y. Yoon, *Nature* **1978**, *272*, 226.
[10] A. Peterlin, *J. Mat. Sci.* **1971**, *6*, 490.
[11] A. Galeski, Z. Bartczak, A. S. Argon, R. E. Cohen, *Macromolecules* **1992**, *25*(21), 5705.
[12] A. Galeski, A. S. Argon, R. E. Cohen, *Macromolecules* **1991**, *24*(13), 3953.
[13] H. H. Song, A. S. Argon, R. E. Cohen, *Macromolecules* **1990**, *23*(3), 870.
[14] A. Bellare, R. E. Cohen, A. S. Argon, *Polymer* **1993**, *34*(7), 1393.
[15] Z. Bartczak, A. Galeski, A. S. Argon, R. E. Cohen, *Polymer* **1996**, *37*(11), 2113.
[16] L. Lin, A. S. Argon, *Macromolecules* **1992**, *25*(15), 4011.
[17] G. Machado, E. L. Denardin, E. J. Kinast, M. C. Gonçalves, M. A. de Luca, S. R. Teixeira, D. Samios, *European Polymer Journal* **2005**, *41*, 129.
[18] R. J. Young, P. B. Bowden, J. M. Ritchie, J. G. Rider, *J. Mat. Sci.* **1973**, *8*, 23.
[19] Z. Bartczak, A. S. Argon, R. E. Cohen, *Macromolecules* **1992**, *25*(19), 5036.
[20] A. D. Drozdov, R. K. Gupta, *Int. J. Eng. Sci.* **2003**, *41*(20), 2335.
[21] M. F. S. Lima, M. A. Z. Vasconcellos, D. Samios, *J. Polym. Sci. Part B: Polymer Physics* **2002**, *40*, 896.

 

[22] S. Tokumoto, D. Samios, A. L. D. Bragança, BR Patent deposit MU7903031-9, 12.24.1999. DEINPI/RS-Brazil (1999).
[23] S. Tokumoto, ''*Deformação Plástica do Polipropileno Isotático: Aspectos do Mecanismo, Propriedades e Morfologia*'', Ph.D. thesis, Federal University of Rio Grande do Sul, Brazil, 2003.
[24] R. C. Spencer, *J. Appl. Phys.* **1949**, *20*, 413.
[25] E. P. Moore, Jr., ''Polypropylene Handbook'' in: *Structure and Morphology*, R. A. Phillips, M. D. Wolkowicz, Eds., Hanser, New York, NY 1996, Chap. III, p. 113.
[26] B. Wunderlich, ''*Macromolecular Physics, vol. 1: Crystal Structure, Morphology, Defects*'', Academic Press, New York 1973.
[27] P. J. Flory, ''*Principles of Physical Chemistry*'', Cornell University Press, Ithaca, NY 1975.
[28] P. J. Flory, *J. Macromol. Sci. Phys.* **1976**, *B12*, 1.
[29] H. Benoit, *J. Macromol. Sci. Phys.* **1976**, *B12*, 27.
[30] G. D. Wignoll, G. H. Ballard, J. Schelten, *J. Macromol. Sci. Phys.* **1976**, *B12*, 75.
[31] E. W. Fischer, J. H. Wendorff, M. Detternmaier, G. Lieser, I. Voight-Martin, *J. Macromol. Sci. Phys.* **1976**, *B12*, 41.
[32] A. Marigo, C. Marega, E. Zannetti, R. Zannetti, *Makromol. Chem.* **1991**, *192*, 523.
[33] V. Caldas, G. R. Brown, R. S. Nohr, J. G. McDonald, L. E. Raboin, *Polymer* **1994**, *35*, 899.
[34] N. S. Murthy, H. Minor, C. Bednarczyk, Krimm, *Macromolecules* **1993**, *26*, 1712.
[35] R. Hosemann, W. Wilke, *Makromol. Chem.* **1968**, *118*, 230.
[36] Z. Mencik, *J. Macromol. Sci. Phys.* **1972**, *B6*(1), 101.

 